

submitted to the Astronomical Journal

Molecular Gas and Star Formation in NGC 3077

David S. Meier and Jean L. Turner

Department of Physics and Astronomy, University of California, Los Angeles, CA 90095-1562
email: meierd;turner@astro.ucla.edu

and

Sara C. Beck

Department of Physics and Astronomy, Tel Aviv University, Ramat Aviv, Israel
email:sara@wise.tau.ac.il

ABSTRACT

We present high resolution ($\sim 2.''5$) CO(1-0) and CO(2-1) images of the central kiloparsec of NGC 3077 made with the Owens Valley Millimeter Array. CO emission is distributed in three major complexes which resolve into at least seven GMCs. Two complexes are associated with the central starburst. A third, more distant complex is not associated with strong star formation. The GMCs are ~ 70 pc in size and contain $\sim 10^6 M_\odot$ of molecular gas. The Galactic conversion factor appears applicable to NGC 3077, consistent with its solar metallicity. Galactic rotation in NGC 3077 is detected for the first time in the molecular gas. The molecular gas counterrotates with respect to the large scale HI tidal bridge. The molecular clouds closest to the starburst have super-virial linewidths, possibly related to the turbulence generated by the starburst. The 2.6 mm radio continuum flux indicates that thermal Bremsstrahlung dominates the emission from the starburst region below 5 cm, and that the $N_{Lyc} \simeq 3.7 \times 10^{52} s^{-1}$ or ~ 3000 O7 stars, corresponds to a star formation rate of $0.4 M_\odot yr^{-1}$. At this rate the amount of molecular gas can sustain star formation for only ~ 10 Myrs; thus NGC 3077 is a true starburst galaxy. The derived age of the starburst is consistent with the inferred ages of the superbubbles, which suggests that the burst is much younger than the age of the M 81-M 82-NGC 3077 interaction. We suggest that it is caused by gas that was pulled out of NGC 3077 during the interaction with M 81, raining back down onto the galaxy.

Subject headings: galaxies:dwarf—galaxies:individual(NGC 3077)—galaxies:ISM —galaxies:nuclei—galaxies:starburst—galaxies:star clusters

1. Introduction

Localized star formation in dwarf galaxies can be as intense as that in large spiral galaxies. Dwarf starburst galaxies appear to have some of the most dramatic examples of “super-star-cluster” formation (eg. O’Connell, Gallagher, & Hunter 1994; Meurer et al. 1995; Maoz et al. 1996). However dwarf galaxies do not contain the usual triggering mechanisms believed to operate in large spirals, such as spiral arms or bars. Many young starbursts in dwarfs (especially the galaxies characterized by Wolf-Rayet emission) seem to have been triggered by tidal/interaction events (Beck 2000). Possible perpetrators of these interaction episodes are massive spirals, dwarfs or even intergalactic gas clouds. The impact of these interactions on the gas can have important consequences on the nature and mode of star formation. NGC 3077 is a nearby example of a galaxy that has experienced a strong tidal interaction in the recent past and is now in a starburst phase.

NGC 3077 is the somewhat overlooked third member of the widely-studied and closest group of strongly interacting galaxies, the M 81 system ($D = 3.9$ Mpc; Table 1). The morphological classification of NGC 3077 is ambiguous, perhaps due to its recent interaction with the of the members of the group, M 81 and M 82. Signs of interactions between the galaxies are well established. Large HI streamers/bridges connect NGC 3077 to M 81. In addition, there is an extended ridge of atomic gas southeast of NGC 3077’s nucleus with more HI than found in the galaxy nucleus itself (Cottrell 1976; van der Hulst 1979; Appleton, Davies, & Stephenson 1981; Yun, Ho, & Lo 1994; Walter & Heithausen 1999; Walter et al. 2001b). While M 82, the other dwarf interacting with M81, has gotten most of the attention, NGC 3077 is also undergoing a burst of recent star formation (Barbieri, Bertola, & di Tullio 1974; Price & Gullixson 1989; Thronson, Wilton, & Ksir 1991). The total atomic mass content near NGC 3077 ($M_{HI} \sim 5 \times 10^8 M_{\odot}$) is similar to that found in M 82 (Cottrell 1976; van der Hulst 1979; Walter et al. 2001b; Crutcher, Rogstad & Chu 1978; Yun, Ho, & Lo 1993). Unlike M 82 though, the majority of the atomic gas is outside the optical confines of the galaxy (Walter & Heithausen 1999; Walter et al. 2001b). Moreover, the total molecular gas content differs by nearly two orders of magnitude (eg. Young & Scoville 1984; Becker, Schilke, & Henkel 1989). The cause of these differences are not well understood. In fact, numerical models have yet to reach consensus whether the gas stripped out of a previously gas-rich NGC 3077 or stolen from M 81 during the interaction (Cottrell 1976; van der Hulst 1979; Brouillet et al. 1991; Donner & Thomasson 1993; Thomasson & Donner 1993; Yun, Ho, & Lo 1994; Yun 1998)

Lower resolution CO studies of NGC 3077 show that it contains a large molecular cloud complex ($\sim 10^7 M_{\odot}$) at its center (Becker, Schilke, & Henkel 1989; Thronson & Carlstrom 1992). It is probably this molecular cloud complex that provides the fuel for the current starburst event. The goal of this paper is to map out the molecular complex at high resolution in CO(1-0) to look for further clues on how the starburst in NGC 3077 has proceeded, and to access the validity of the galactic conversion factor in this metal rich dwarf. Also simultaneous observations of CO(2-1) are used to determine molecular gas temperatures and densities.

2. Observations

Simultaneous aperture synthesis observations of the CO(1-0) transition (115.271 GHz) and the CO(2-1) transition (230.538 GHz) were made with the Owens Valley Radio Observatory (OVRO) Millimeter Interferometer between 1997 October 12 and 1997 December 09 (Table 2). The interferometer consists of six 10.4 m antennas with cryogenically cooled SIS receivers (Padin et al. 1991; Scoville et al. 1994). System temperatures (single sideband) ranged from 400 - 1800 K at 115 GHz and 500 - 1100 K at 230 GHz. A 64 channel, 2 MHz filterbank was used to cover each transition. This gives a velocity resolution of 5.2 km s^{-1} (2.6 km s^{-1}) for CO(1-0) (CO(2-1)), corresponding to an overall bandwidth of 333 km s^{-1} (166 km s^{-1}). The CO(2-1) data have been smoothed to 5.2 km s^{-1} to increase S/N and to match the velocity resolution of CO(1-0). The systemic velocity (LSR) was set to be 7.0 km s^{-1} centered at channel 32.5. Two pointings with phase centers of $\alpha_1(\text{B1950}) = 09:59:20.0$; $\delta_1(\text{B1950}) = 68:58:34.0$, $\alpha_2(\text{B1950}) = 09:59:18.3$; $\delta_2(\text{B1950}) = 68:58:40.0$, were mosaicked to cover the nuclear starburst. The data were calibrated using the MMA software package. Phase calibration was done by observing the quasars 1044+719 and 0923+392 every 20 minutes. Absolute flux calibration was done using Neptune and Uranus as primary flux calibrators and 3C273 as secondary flux calibration. Tracking variations in the measured flux of 3C273 with time implies that absolute fluxes are good to 10% at 3 mm and 20% at 1 mm.

The two pointings were mosaicked using the MIRIAD software package. The maps are naturally weighted and primary-beam corrected. The OVRO primary beam is $\sim 64''$ at (1-0) and $\sim 34''$ at (2-1). Since the maps are mosaics, the noise level varies across the maps. The noise increases towards the edge of the field both because of the decreased sensitivity due to the primary beam and due to a factor of ~ 2 less integration time. Reported noise levels for this paper are those measured from line free regions of the map half-way between the map center and the FWHM points. The noise level is a bit lower than this in the center ($\sim 10\%$) and somewhat higher than this towards the edges of the map ($\sim \sqrt{2}$). All further data reduction, analysis and manipulation was done using the NRAO AIPS package.

The shortest baselines sampled in the dataset are $\simeq 15 \text{ m}$. This corresponds to spatial scales of $\sim 36''$ for (1-0) and $\sim 18''$ for (2-1). Structures extended on scales larger than this will be resolved out by the interferometer. The amount of flux resolved out has been estimated by convolving both maps to the resolution of the single-dish data (Becker, Schilke, & Henkel 1989). The peak CO(1-0) (CO(2-1)) intensities in the OVRO maps, when convolved to a $21''$ ($13''$) beamsize are 3.0 K km s^{-1} (3.8 K km s^{-1}). We therefore detect $\sim 80\%$ ($\sim 60\%$) of the peak intensities obtained from the single-dish observations.

3. Results

3.1. Molecular Gas Morphology

The CO channel maps of NGC 3077 are presented in Figures 1-2. Emission is detected in channels from $V_{LSR} = -30$ to $+30$ km s $^{-1}$ with peak antenna temperatures of ~ 3.0 K for CO(1-0) and 1.9 K for CO(2-1) (Table 3). Integrated intensity maps are plotted to the same scale in Figure 3. The molecular gas is concentrated into three major complexes, consistent with what is seen in lower resolution images (Thronson & Carlstrom 1992). The central two complexes are extended northeast-southwest along the major axis of the galaxy (p.a. $\sim 45^\circ$; Table 1). The third complex is found ~ 550 pc in projection from the center of NGC 3077, northwest along the minor axis.

Figure 4 shows the CO(1-0) integrated intensity map overlaid on HST images of the galaxy in infrared and UV light (Maoz et al. 1996; Böker et al. 1999). Near-infrared continuum emission is likely dominated by older stellar populations, so we use the NICMOS H band image (Figure 4a) to locate the dynamical center of the galaxy (assumed to be the centroid of the old stellar population). The brightest of the molecular gas complexes, GMCs B + D (§3.1.1), is within $3''$ of the H band centroid. The strongest star forming region, as traced by 2.6 mm continuum (§3.2) and P α (Figure 4b), is located at the interface of these two GMCs and is labeled “*” in Figure 3. Weaker star formation is seen towards the northeastern complex, GMC A.

The correspondence between the central molecular gas distribution and the extinction seen in the HST FOC UV image (Figure 4c) is striking. This strongly suggests that the youngest star forming regions are obscured by the dust associated with the molecular clouds. The two clusters seen in the UV (UV1 and UV2) are presumably older than the starburst cluster, having cleared out much of their molecular gas. The southwestern UV cluster, UV2, is found at the base of the large superbubble seen in H α and P α (eg. Martin 1998; Böker et al. 1999, Figure 4a), indicating that it may be the energy source of the superbubble. Very recently, high resolution HI observations of NGC 3077 have been presented and show that HI and the superbubbles tend to be anti-correlated (Walter et al. 2001b).

3.1.1. Giant Molecular Clouds in NGC 3077

Because of its higher sensitivity and slightly higher effective critical density, the CO(2-1) data are used to fit the properties of the GMCs. Each cloud, identified as a region of spatially and spectrally localized emission but not necessarily a gravitationally bound entity, has been fit with an elliptical Gaussian to determine its size, location, and intensity. Three molecular clouds lie outside the (2-1) primary beam. Of these, only GMC F was fit using the CO(1-0) data since GMC E & G are weak or at the edge of the (1-0) primary beam. Once cloud sizes were determined, a box containing all the emission from the cloud was summed to produce a spectrum. This spectrum was then fit with a gaussian to obtain its linewidth.

All of the fitted GMCs have been resolved except GMC C (Table 4). The three central GMCs A, B, and D are ~ 70 pc in size, with implied virial masses of about $10^{6-7} M_{\odot}$ and FWHM linewidths of 25 - 50 K km s^{-1} (Table 4). These GMCs are similar or slightly larger in size to those in other dwarf galaxies (eg. Rubio, Lequeux, & Boulanger 1993; Wilson 1994, 1995; Taylor et al. 1999; Walter et al. 2001a), and consistent with the larger GMCs seen in nearby spirals (eg. Solomon et al. 1987; Vogel, Boulanger, & Ball 1987; Wilson & Scoville 1990; Wilson & Rudolph 1993; Meier & Turner 2001). On the other hand, the linewidths of the clouds in NGC 3077 are larger than seen in other dwarf galaxies. Typical FWHM linewidths found for ~ 70 pc GMCs in nearby dwarfs are ~ 10 km s^{-1} (eg. Wilson 1994; Taylor et al. 1999; Walter et al. 2001a), whereas in NGC 3077 they are 25 - 50 km s^{-1} . It is possible that these GMCs are made of smaller unresolved clumps. In such a case, the linewidths of the individual clumps will be smaller, and our measured linewidths will reflect the random motions of the clumps in the GMC. Using the derived rotation curve (§3.1.2), we estimate that the contribution of galactic rotation to the linewidth is at most 5 km s^{-1} . The two GMCs with the largest linewidths are GMC B & D. These GMCs are the ones most closely associated with the starburst. GMC F, well away from the starburst, does have a linewidth that is much smaller, and similar to what is found for the other dwarfs. Masses estimated assuming that these GMCs are in virial equilibrium are compared with masses estimated by other means in §4.2. The masses estimated assuming virialization holds tend to be larger than found by other methods. This fact implies that at the burst GMCs additional contributions to the linewidth besides gravitation may be present.

3.1.2. The Velocity field

Figure 5 displays the velocity field (moment 1) and the velocity dispersion (moment 2) maps derived from the CO(1-0) dataset (the CO(2-1) velocity field, not shown, is similar to CO(1-0)). While only a limited portion of the total HI velocity field can be traced with CO, it appears that galactic rotation is detected for the first time in the molecular gas. Though small deviations are seen, the velocity field is consistent with solid body rotation with $v_{LSR} \simeq 5$ km s^{-1} and a total range of ± 30 km s^{-1} over the central $20''$ radius along a p.a. of $\sim 45^\circ$, similar to the optical major axis (Figure 5 insert). Galactic rotation is ~ 1.3 $\text{km s}^{-1} \text{ arcsec}^{-1}$, or ~ 68 $\text{km s}^{-1} \text{ kpc}^{-1}$ (corrected for an inclination of 45°).

The sense of rotation of the CO velocity field is *opposite* of what is seen in HI (Cottrell 1976; van der Hulst 1979; Walter et al. 2001b). In CO, the blueshifted side of the galaxy is in the northeast, whereas in HI the blueshifted side is the southwest (though there some evidence for a reversal of the HI velocity field towards the very center of the galaxy — Figure 12 of van der Hulst 1979; Walter et al. 2001b). One possible explanation for this reversal is that the four GMCs that dominate the central emission are rotationally decoupled from the rest of the galaxy. A second possibility is that the velocity field traced by the HI is not representative of the true rotation of NGC 3077. van der Hulst (1979) has suggested that the velocity field seen in the atomic gas

appears to smoothly trace that of the tidal bridge connecting NGC 3077 to M 81, and hence the galactic rotation of NGC 3077 may not be separable from the bulk motions of the tidal tail. Optical spectroscopy, like CO, suggests that the blueshifted nebular velocities are in the northeast (Barbieri, Bertola, & di Tullio 1974). We feel that the CO velocity field probably reflects galactic rotation and large beam HI observations do not. The velocity of the third major CO complex, (GMCs F & G), located along the minor axis, has a line center velocity of -22 km s^{-1} . This is substantially blueshifted ($\Delta v \simeq -30 \text{ km s}^{-1}$) relative to what would be expected from a rotating disk with the CO velocity field. This suggests that the cloud complex is either falling in towards or expanding out from the nucleus.

3.2. Millimeter Continuum Emission

Observations of continuum emission at 2.6 mm and 1.3 mm have been made for NGC 3077. 2.6 mm continuum is detected and Figure 6 shows the 2.6 mm continuum map generated with a $75\text{k}\lambda$ tapered (beamsize $3.''9 \times 3.''8$, $pa = -79^\circ$; Table 2). 1.3 mm continuum emission is not convincingly detected at any location, with a 3σ upper limit of $9.5 \text{ mJy beam}^{-1}$. The 2.6 mm continuum peaks between GMCs B & D, consistent within the uncertainties with the dominant nebula seen in $P\alpha$. A possible weaker source is seen towards the UV cluster, UV2. The peak intensity of the starburst is $3.1 \pm 0.7 \text{ mJy beam}^{-1}$ (as measured in the $2.''5$ untapered map). The emission is slightly resolved. The total 2.6 mm flux summed over the central $10''$ (190 pc) centered on the starburst cluster marked by “*” in Figure 3 is $8.0 \pm 2.0 \text{ mJy}$. The morphology is consistent with the higher resolution and sensitivity 20 cm VLA map of the nucleus (Hummel et al. 1987). Hummel et al. (1987) find that the central cluster has a flux of $3.6 \pm 0.3 \text{ mJy}$ at 1.46 GHz over a deconvolved size of $11 \text{ pc} \times 6 \text{ pc}$. The spectral index, α ($S_\nu \propto \nu^\alpha$), found for the central cluster between 2.6 mm and 20 cm is $\alpha_{0.26}^{20} \simeq -0.03 \pm 0.08$. This flat spectral index demonstrates that the radio emission from the central starburst HII region is dominated by thermal Bremsstrahlung emission out to 1.4 GHz. Single-dish observations of the central region of NGC 3077 ($2.''7$ beam at 5 cm and $1.''2$ beam at 2.8 cm), obtain fluxes of $22 \pm 8 \text{ mJy}$ at 5 cm (Sramek 1975) and $13 \pm 1 \text{ mJy}$ at 2.8 cm (Niklas et al. 1995). These fluxes give spectral indices of $\alpha_{0.26}^5 \simeq -0.34 \pm 0.20$ and $\alpha_{0.26}^{2.8} \simeq -0.20 \pm 0.15$, respectively. Evidently, the radio fluxes detected in these large beams are also predominately thermal emission and are dominated by the central $10''$ of the galaxy. Beyond 5 cm, synchrotron emission becomes a significant contributor to the radio flux.

4. Discussion

4.1. Physical Conditions of the Molecular Clouds in NGC 3077

Changes in the physical conditions of the molecular gas can be traced using the CO(2-1)/CO(1-0) ratio. When opacities are large, the CO(2-1)/CO(1-0) ratio is just the ratio of the Rayleigh-Jeans

corrections at the two frequencies, and hence is moderately temperature sensitive (eg., Braine & Combes 1992). The physical condition of the molecular gas in dwarf galaxies is of interest because they may be responsible for some portion of the observed differences in X_{CO} , molecular gas abundances and star formation properties between dwarfs and spirals (Israel et al. 1986; Maloney & Black 1988; Elmegreen 1989; Sakamoto 1996). Gas properties in dwarf galaxies such as density, temperature and opacity appear not to differ significantly on large scales (Sage et al. 1992; Meier et al. 2001), but this is not well established yet. Physical conditions of the gas in dwarf galaxies, including NGC 3077, have been addressed elsewhere (Meier et al. 2001). In this section we focus on new insights gained from these higher resolution images.

The CO(2-1)/CO(1-0) ratio for both the peak antenna temperatures, T_{mb}^{pk} , and integrated intensities of each GMC are displayed in Table 3. GMCs B & D both have ratios ~ 0.6 , while GMC A has a slightly higher ratio of ~ 0.82 . These values are somewhat lower than are common for starburst regions (Braine & Combes 1992), but are consistent with those of Galactic GMCs, and of nearby, less active dwarf galaxies (Sage et al. 1992; Sakamoto et al. 1997; Oka et al. 1998; Barone et al. 2000). The T_{mb}^{pk} ratios do not peak at the exact location of the starburst in NGC 3077, unlike what is seen in the other nearby starbursts like M 82 (Weiss et al. 2001), IC 342 (Meier & Turner 2001) and Maffei 2 (Meier, Hurt, & Turner 2001). Ratios of 0.6 - 0.8 imply an excitation temperature, T_{ex} of 5 - 10 K for the clouds. Comparing T_{ex} to T_{mb}^{pk} , for each cloud provides an estimate of the GMCs areal filling factor, $f \simeq T_{mb}^{pk}/T_{ex}$. Typical values of the filling factors are 0.5 for the HII region GMCs (B & D) and 0.2 for GMC A. Unlike the T_{mb}^{pk} ratios, the CO(2-1)/CO(1-0) integrated intensity ratios *do* peak towards GMC D near the starburst site. The difference between the integrated line ratio and the T_{mb}^{pk} ratio is explained by the CO(2-1) spectral line being wider than the CO(1-0) line in this region. The CO(3-2) linewidth shows the same trend (Meier et al. 2001).

Since the amount of flux resolved out by the interferometer differs for the two transitions, the observed ratios will differ from the true ratios by factors up to the ratio of the differences in resolved out flux, 30%, depending on the distribution of the resolved flux. This effect should be less dramatic for ratios of T_{mb}^{pk} since the brightest regions of emission are generally localized in clouds. Therefore, the ratio of T_{mb}^{pk} are likely better representations of the true ratio than ratios of integrated intensities, but are still lower limits. Since the amount of resolved out flux is greater at CO(2-1) than at CO(1-0), the diffuse component resolved out by the interferometer appears to have a ratio larger than 1, suggestive of optically thin gas. The single-dish CO(3-2)/CO(1-0) line ratio of 1.1 for NGC 3077 is one of the largest measured for dwarf starbursts (Meier et al. 2001), so it is not unreasonable to expect some optically thin CO emission.

A sample of Large Velocity Gradient (LVG) radiative transfer models were run to relate the observed T_{mb}^{pk} and ratios to the intrinsic cloud properties of density, n_{H_2} , and kinetic temperature, T_k (Goldreich & Kwan 1974; Scoville & Solomon 1974; de Jong et al. 1975). Details of the LVG model used can be found in Meier et al. (2001). In Figure 7, two models are displayed with $X_{CO}/dv/dr = 10^{-4.1}$ and $X_{CO}/dv/dr = 10^{-4.5}$ for the three central GMCs. These abundance

per velocity gradients are based on the solar neighborhood CO/H₂ abundance (8×10^{-5} ; Frerking, Langer, & Wilson 1982) and a velocity gradient, $dv/dr \sim 1 \text{ km s}^{-1}$ (Table 4).

Best fit solutions obtained from the LVG modeling give $\langle n_{H_2} \rangle \sim 200 \text{ cm}^{-3}$ and $T_k \gtrsim 25 \text{ K}$ for the three central GMCs. Cooler and denser solutions are also permitted for GMCs A and B ($\langle n_{H_2} \rangle \gtrsim 10^3 \text{ cm}^{-3}$ and $T_k \sim 10 - 20 \text{ K}$). Little difference is found between the two solutions with different $X_{CO}/dv/dr$. Changing the estimated filling factors substantially from the assumed values worsen the χ^2 fits. Increasing the filling factor by a factor of two pushes the best fit solutions to slightly cooler ($\Delta T_k \sim 5 \text{ K}$) and denser ($\langle \Delta n_{H_2} \rangle \sim 0.3 \text{ dex}$) solutions. Since the ratios are lower limits due to the differences in resolved out flux between the two transitions, the true gas densities and temperatures are likely to be higher than the above values. Single-dish LVG modeling using CO(3-2) data do, in fact, obtain higher gas temperatures and densities ($T_k \gtrsim 20 \text{ K}$, $\langle n_{H_2} \rangle \gtrsim 10^3 \text{ cm}^{-3}$; Meier et al. 2001). Therefore, while not dramatic, indications of elevated kinetic temperatures are present.

4.2. The Conversion Factor in NGC 3077

To study the relationship between molecular gas, dynamics, and star formation one must have an accurate accounting of the amount of molecular gas. Usually N_{H_2} is estimated from I_{CO} using a conversion factor, X_{CO} , which is empirically determined from Galactic molecular clouds. There is evidence that X_{CO} can vary. In nuclear starburst regions, the intense radiation field and the different cloud conditions due to the deep potential well can have significant effects on X_{CO} (Maloney & Black 1988; Elmegreen 1989; Sakamoto 1996). While dynamical influences on the conversion factor are expected to be less important in dwarf galaxies, their low metallicities cause CO to be difficult to detect (Israel 1986; Arnault et al. 1988; Verter & Hodge 1995; Wilson 1995; Arimoto, Sofue, & Tsujimoto 1996). The fact that NGC 3077 is a low mass dwarf with solar metallicity (Heckman 1980; Martin 1997; Sakai & Madore 2001) and strong star formation makes it an interesting object in which to estimate the conversion factor.

Molecular masses estimated using the Galactic disk conversion factor, $X_{CO_{gal}} = 2.3 \times 10^{20} \text{ cm}^{-2} (\text{K km s}^{-1})^{-1}$ (Strong et al. 1988; Hunter et al. 1997), are:

$$M_{mol} = 1.23 \times 10^4 (M_{\odot}) D_{mpc}^2 S_{CO}, \quad (1)$$

(eg. Wilson et al. 1988), where S_{CO} is the CO(1-0) flux in Jy km s⁻¹. Derived masses for the GMCs using X_{CO} are shown in Table 4.

To access the applicability of the Galactic conversion factor to NGC 3077, we attempt to estimate the amount of molecular gas independently of X_{CO} . Several methods exist to estimate molecular gas masses, independent of CO(1-0). Since the GMCs in the center of NGC 3077 are resolved, the total mass of the GMCs can be estimated from the virial theorem made with the assumption that they are virialized (eg. Meier & Turner 2001; Meier et al. 2001). The virial cloud

masses assuming $r \propto \rho^\gamma$ with $\gamma = 1$, appropriate for Galactic clouds (eg., Cernicharo, Bachiller, & Duvert 1985; Scoville et al. 1987; MacLaren, Richardson, & Wolfendale 1988), are displayed in Table 4. In general, masses obtained from the virial theorem are larger than those obtained from the CO(1-0) conversion factor. This is particularly evident for GMCs B & D, where the mass derived from the virial theorem is an order of magnitude larger than that from the CO conversion factor. This stems directly from the fact that the clouds have large and possibly nonequilibrium linewidths at these locations (§3.1.2). The virial mass of the most distant GMC, F, is in better agreement with the conversion factor estimate there.

Optical extinction can also be used to estimate the total gas mass present towards the starburst. The extinction to the central starburst is derived by comparing the H α flux of the starburst to the extinction-free millimeter continuum (§4.3), and is found to be $A_V \simeq 2.5$. If it is assumed that the starburst is in the middle of the cloud, then a total extinction of 5 mag is estimated. Assuming that $N_{H_2} \simeq 1 \times 10^{21} \text{ cm}^{-2} \text{ mag}^{-1} A_V$ (eg. Bohlin, Savage, & Drake 1978), a total column density of $N_{H_2} \simeq 5 \times 10^{21} \text{ cm}^{-2}$ is implied. Whereas, the average CO(1-0) intensity at the same location is $\sim 45 \text{ K km s}^{-1}$. From these results a conversion factor of $X_{CO} \sim 1.1 \times 10^{20} \text{ cm}^{-2} (\text{K km s}^{-1})^{-1}$ is estimated. This is slightly smaller but within a factor of two of the Galactic value.

Gas masses can also be estimated from thermal dust emission. For a dust temperature of 34 K (Melisse & Israel 1994), a 1.3 mm dust absorption coefficient of $3.4 \times 10^{-3} \text{ cm}^2 \text{ g}^{-1}$ (Pollack et al. 1994) and a gas-to-dust ratio of 100, $M_{gas} \simeq 1.15 \times 10^5 S_{mJy}(1.3mm) M_\odot$. If we assume that all 1.3 mm flux is due to dust emission (an upper limit since some thermal bremsstrahlung will still contribute), the 3σ upper limit of 10 mJy beam $^{-1}$ equates to $\sim 10^6 M_\odot$. Therefore, unless the nature and emissivity of the dust in NGC 3077 is substantially different from what is found for the Galaxy, the gas masses implied by the dust emission are also significantly lower than the virial values and more in line with the extinction values. So we find that, in general, the dust emission also favors the lower values of the conversion factor.

In this context, the two GMCs (B & D) with the largest “virial” masses appear not to be in virial equilibrium. These two clouds are the closest to the dynamical center and the starburst, and have unusually large linewidths for their sizes (§3.1.1). Additional evidence that these clouds are not virialized can be seen by comparing the densities implied by the virial mass with those estimated from gas excitation (LVG modeling; Figure 7). The dot-dashed line represents the beam-averaged molecular cloud density implied by the virial theorem. In the case of GMC D, the beam-averaged value is a factor of two larger than any acceptable parameter space allowed from the LVG analysis and a factor of six larger than the optimal solution. For GMCs A & B, there is strictly speaking some overlap with regions of acceptable parameter space but they are again much denser than the optimal LVG solution (§4.1). If these GMCs resolve into smaller clumps then these clumps appear to move around at velocities greater than virialization suggests. Detailed studies of the nearby starburst spirals, IC 342 and Maffei 2, also show that the GMCs also have super-virial linewidths (eg. Meier & Turner 2001; Meier, Hurt, & Turner 2001). Significant non-circular motions due to barred potentials are likely the cause of the large linewidths in these two spiral galaxies, but such

motions cannot be the cause in NGC 3077. The increased linewidths indicate that these GMCs associated with the starburst have a higher level of turbulence, possibly from shocks due to star formation, cloud-cloud collisions, or the mechanical energy input from the associated superbubbles (Martin 1998).

In summary, the above methods imply that the CO conversion factor applicable to NGC 3077 is approximately equal to or slightly lower than the Galactic value of $2.3 \times 10^{20} \text{ cm}^{-2} (\text{K km s}^{-1})^{-1}$. Since NGC 3077 is roughly solar metallicity, this is reasonable.

4.3. The Star Formation Rate in NGC 3077

At millimeter wavelengths synchrotron emission is weak and the radio continuum emission for normal galaxies is dominated by optically thin free-free emission or dust emission. Dust emission is weak at 1.3 mm (§3.2), and hence should not be a significant contaminant to the 2.6 mm continuum emission. Therefore 2.6 mm provides an excellent estimate of the Lyman continuum flux and the strength of massive star formation. We use our 2.6 mm continuum detection to make an extinction-free estimate of the strength of the starburst in NGC 3077. The number of Lyman continuum photons implied by the 8.0 mJy of 2.6 mm continuum is $N_{Lyc} \simeq 3.7 \pm 0.8 \times 10^{52} \text{ s}^{-1}$ over the central $10''$. We detect $N_{Lyc} \simeq 1.4 \pm 0.4 \times 10^{52} \text{ s}^{-1}$ from the central starburst cluster alone (assuming $T_e = 10^4 \text{ K}$, eg. Mezger & Henderson 1967). This is about six times the strength of 30 Dor (eg. Vacca et al. 1995). The number of effective O7 stars needed to produce this N_{Lyc} is ~ 3000 ($L_{O7} \simeq 7.4 \times 10^8 L_\odot$), of which ~ 1000 ($L_{O7} \simeq 2.8 \times 10^8 L_\odot$) come from the central cluster (Vacca, Garmany, & Shull 1996). Clearly, to explain the bright 2.6 mm continuum flux, a large amount of young, massive stars must have been forming over the last $\sim 10 \text{ Myr}$.

N_{Lyc} derived from the $H\alpha$ flux is $5.3 \times 10^{51} \text{ s}^{-1}$ (Price & Gullixson 1989; Thronson, Wilton, & Ksir 1991; Martin 1997), a factor of seven lower than predicted from the 2.6 mm data. Extinction is almost certainly the cause of most of the difference. Comparison of the millimeter and the $H\alpha$ rate implies an average extinction at $H\alpha$ of 2.1 mag, or $A_V = 2.5 \text{ mag}$ (assuming $A_\lambda \propto \lambda^{-1}$). The $P\alpha$ flux measured over the same region (Figure 4b) is also consistent with an A_V of 2.5 - 3.0 mag (Böker et al. 1999; Walter et al. 2001b). The star formation rate (SFR) derived from $H\alpha$ luminosity is $\sim 0.06 M_\odot \text{ yr}^{-1}$ (eg. Thronson, Wilton, & Ksir 1991). Corrected for extinction, the implied true SFR is $0.4 M_\odot \text{ yr}^{-1}$ over the central 190 pc. This equals the SFR predicted from the FIR Luminosity (eg. Thronson, Wilton, & Ksir 1991, Table 1); the luminosity derived above from the number of O stars also equals the observed far-infrared luminosity. This argues that all of the FIR luminosity comes from light reradiated from the starburst population; other possible FIR sources such as cirrus and dust heated by the old stellar population do not appear to contribute significantly (eg. Bothun, Lonsdale, & Rice 1989; Thronson, Wilton, & Ksir 1991).

Assuming the conversion factor in NGC 3077 is similar to the solar neighborhood (§4.1), there is $4.5 \times 10^6 M_\odot$ of molecular gas over the central $10''$ (corrected for resolved out flux). If the CO

rotation curve accurately traces the dynamics of NGC 3077 over this region (§3.1.2), a dynamical mass of $\sim 9.7 \times 10^6 M_\odot$ obtained. This implies a molecular mass fraction of $\sim 50\%$ over the central 200 pc radius. This large molecular mass fraction is similar to what is found for nuclei of nearby starburst spirals, including M 82, but it is substantially larger than is typical for dwarf galaxies or ellipticals (Young & Scoville 1984; Scoville et al. 1991; Young & Devereux 1991; Turner 1994; Wiklind, Combes, & Henkel 1995; Solomon et al. 1997). Even a factor of two overestimate in the amount of molecular gas, would imply a molecular mass fraction of $\sim 25\%$, which is still high for dwarfs.

Even with a relatively large molecular mass fraction, the star formation in NGC 3077 is unusually vigorous for its molecular mass. Rownd & Young (1999) find $\frac{L_{\text{H}\alpha}}{M_{\text{H}_2}}$ in NGC 3077 to be one of the largest seen in nearby galaxies. In their sample of 121 (mostly spiral) galaxies only NGC 1569 (whose molecular mass is probably underestimated due to its low metallicity; Taylor et al. 1999) and NGC 3310 have higher values. Given the amount of molecular gas and the derived star formation rate, the central molecular cloud complex can support star formation for only ~ 11 Myr. The several superbubbles in H α are further evidence for a shortlived starburst (Martin 1998). The mechanical power of a wind driven superbubble gives an age of $\lesssim 10$ Myr for the superbubbles, Martin (1998), and presumably the starburst, in NGC 3077. Therefore, it seems plausible that the current starburst epoch started around 10 Myrs ago.

The UV clusters near GMC A have weak or no 2.6 mm continuum associated with them and only weak P α emission. These clusters that are not embedded in molecular gas are probably somewhat older than those seen at the interface of GMCs B & D. Optical/UV observation of these clusters suggest that they are $\sim 10 - 100$ Myr old with the older age stars increasingly dominating as one proceeds away from the center (Benacchio & Galletta 1981; Price & Gullixson 1989; Abdel-Hamid & Notni 2000a,b; Sakai & Madore 2001).

4.4. The Trigger of the Starburst

In the course of an interaction redistribution of large amounts of gas can occur, often times leading to starbursts in the host galaxies. NGC 3077 is a dramatic example of such tidal carnage, however it is as yet unclear what the source of the gas that has generated these tidal features are and how they relate to the current nuclear starburst. The gas surrounding NGC 3077 either originally belonged to gas-rich disk associated with NGC 3077 that has been stripped out due to the interaction (Yun, Ho, & Lo 1994; Yun 1998), or the gas has been captured from M 81 during its most recent passage (Thomasson & Donner 1993; Donner & Thomasson 1993). In either case, the interaction has had a strong influence on the gas distribution, and probably is responsible at some level for the starburst.

A consideration of the timescales involved provide clues as to how the starburst and the interaction are related in detail. Despite the ambiguity in the source of the neutral gas surrounding

NGC 3077, all simulations of the M 81-M 82-NGC 3077 group agree that the strongest interaction between NGC 3077 and M 81 occurred 300 - 600 Myr ago (Cottrell 1976; van der Hulst 1979; Brouillet et al. 1991; Donner & Thomasson 1993; Thomasson & Donner 1993; Yun, Ho, & Lo 1994; Yun 1998). The strength of the starburst estimated from the 2.6 mm continuum, the superbubble sizes (Martin 1998) and the UV colors (Benacchio & Galletta 1981; Price & Gullixson 1989; Abdel-Hamid & Notni 2000a,b; Sakai & Madore 2001) all suggest that the current burst of star formation is $\lesssim 10$ Myr old. While the star formation of the outer parts of NGC 3077 and its halo object, “Garland”, appear to be $\lesssim 150$ Myrs old, more consistent with a direct trigger by the interaction (Sakai & Madore 2001), the central burst appears too young to have been triggered directly.

Based on considerations of dynamical friction alone, it is expected that gas should rain down on the disk of NGC 3077 for a few Gyrs after closest interaction. Additional evidence for infall can be seen in our CO data: firstly, the starburst appears to be a result of the collision of GMCs B & D, and secondly, the complex of molecular gas comprising GMCs E-G is located along the minor axis of NGC 3077 and is moving with substantial net line-of-sight motion relative to the LSR velocity of the galaxy.

To get an estimate of the relevant dynamical friction timescale for the gas around NGC 3077, we consider the fate of the recently discovered atomic/molecular gas cloud complex ~ 4.8 kpc to the southeast of NGC 3077’s center (Walter & Heithausen 1999; Heithausen & Walter 2000). Walter & Heithausen (1999) suggest that this complex may be a dwarf galaxy forming. Whether this gas cloud (the WH complex) will form a separate dwarf galaxy or will fall back into NGC 3077 depends on the geometry of the system. Despite many attempts, the exact interaction geometry of the M 81-M 82-NGC 3077 system is still not completely understood (Cottrell 1976; Brouillet et al. 1991; Donner & Thomasson 1993; Thomasson & Donner 1993; Yun, Ho, & Lo 1994; Yun 1998), but the models suggest 30° - 50° inclinations with respect to the plane of the sky. Adopting an inclination of 45° and a total mass of NGC 3077 inside the radius of the WH complex of $8.6 \times 10^9 M_\odot$ (Cottrell 1976; van der Hulst 1979), we estimate an escape velocity of 120 km s^{-1} at the location of WH complex. The observed velocity of the WH complex is $\sim 15 \text{ km s}^{-1}$, or only $\sim 10 \text{ km s}^{-1}$ different from the v_{LSR} of NGC 3077, significantly less than the escape velocity. This implies that the WH complex must be moving within $\sim 5^\circ$ of the plane of the sky, if it is to escape NGC 3077’s gravitational potential and become a separate dwarf galaxy.

If the complex is bound to NGC 3077 it will spiral into the nucleus due to dynamical friction. The timescale for a cloud complex to spiral into the center is (eg., pg. 428 Binney & Tremaine 1987; Sparke & Gallagher 2000):

$$\tau_{df} \lesssim \frac{1.17 r_i^2 v_c}{\ln(\Lambda) G M} \simeq \frac{264 \text{ Gyr}}{\ln(\Lambda)} \left(\frac{r_i}{2 \text{ kpc}} \right)^2 \left(\frac{v_c}{250 \text{ km s}^{-1}} \right) \left(\frac{10^6 M_\odot}{M} \right) \quad (2)$$

where r_i is the distance between the cloud and the center of the galaxy, v_c is the orbital speed of the cloud, M is the mass of the cloud and $\ln(\Lambda)$ is the Coulomb logarithm (the natural logarithm

of the ratio of maximum to minimum impact parameters). There is some uncertainty in this value since the WH complex is not likely on a circular orbit. (Strictly speaking, the lower limit in the eq.(2) is due to the fact that this equation applies to stellar systems; since gas is dissipational it can lose angular momentum more quickly. However, internal dissipation in the cloud should not significantly influence the derived timescale since the basic assumption of a test mass used in this calculation should hold over most of the orbit. The dissipational nature of the gas should only become important when the cloud reaches a distance from the nucleus where tidal forces being to disrupt the cloud [~ 100 pc for the WH complex]). We adopt the following values as suitable to the WH complex, $M \simeq 10^8 M_\odot$, $r_i \simeq 4.8$ kpc, $v_c \sim 50$ km s $^{-1}$ (Walter & Heithausen 1999; Heithausen & Walter 2000) and $\ln(\Lambda) \simeq 5$ (where Λ is approximated as r_i divided by the diameter of the cloud; also consistent with the formulation of Binney & Tremaine (1987)). For these values, the implied dynamical fiction timescale is ~ 600 Myrs. This value is about the same as the time since closest approach. Therefore it seems reasonable that large clouds of atomic or molecular gas similar in mass to the WH complex have spiraled into the center of NGC 3077 with time delays consistent with the current burst.

It is also possible that if NGC 3077 had a large disk of gas previous to the interaction, it could have been driven into the nucleus to trigger the burst. Models suggest that strong tidal interactions can set up bar modes that drive gas to the galaxy center (eg. Noguchi 1987; Barnes & Hernquist 1992). However, this scenario is less favorable for two reasons: (1) the timescales for gas inflow are extremely fast (a few dynamical times or less, $\sim 10^7$ Myr; Hernquist 1989), and again would seem to trigger a burst too quickly, (2) There is no indication of a stellar bar, or any strongly disturbed stellar component remaining in NGC 3077. Therefore, we favor recent infall of gas onto the disk of the NGC 3077 as the cause of the current burst. If NGC 3077 did have a large disk of gas as suggest by Yun et al (Yun, Ho, & Lo 1994; Yun 1998), the above points suggest that a burst of star formation starting a few hundred Myrs ago could have been driven. There are indications for this somewhat older stellar population (Abdel-Hamid & Notni 2000a,b; Sakai & Madore 2001). This might provide hints that the gas around NGC 3077 has been stripped from NGC 3077 itself, however this cannot be taken as proof. While important, how the gas arrived outside the optical disk in the first place does not effect the conclusion that the gas is dynamically unstable and is prone to infall on timescales of hundreds of Myrs. It seems quite reasonable that gas clouds raining down onto the disk of NGC 3077 will drive starburst eposides for the next few \sim Gyrs.

There are other examples of infall triggered starbursts, such as the Galactic disk (the high velocity clouds, eg. Wakker & van Woerden 1997), and possibly nearby dwarf starbursts such as NGC 5253 (Turner, Beck, & Hurt 1997; Meier, Turner, & Beck 1998). Like NGC 3077, NGC 5253 is much too far from its putative partner (M 83) to have interacted in the last few Myrs (the age of its starburst). If these starbursts are triggered by the gas accreting back onto the disk from a past interaction, then significant delays can easily be explained. If such a scenario is correct then a dwarf galaxy may not always need a close companion in order for its star formation to be triggered by an interaction event. Smaller clouds of gas ($10^{6-8} M_\odot$) falling back to the galaxy can sustain

bursts of star formation for several Gyrs after closest approach.

5. Summary and Conclusions

Images of NGC 3077 in the lines of CO(2-1) and CO(1-0), obtained from the Owens Valley Millimeter Array, show CO emission in three major complexes. Two of the complexes are associated with the central starburst and the third is along the minor axis at a distance of ~ 0.5 kpc. The three complexes resolve into at least seven GMCs, with diameters of ~ 70 pc and masses of $\sim 10^6 M_\odot$, similar to large GMCs in the Galaxy and in other nearby gas-rich dwarfs. Linewidths of the two GMCs closest to the starburst are quite large, suggesting that either winds, outflows or accretion flows are important in these clouds. Galactic rotation is detected for the first time in the molecular gas. The molecular gas is counterrotating with respect to the large scale HI tidal bridge. Molecular gas makes up ~ 50 % of the dynamical mass in the central $10''$.

The CO(2-1)/CO(1-0) antenna temperature ratio in NGC 3077 ranges from 0.6 - 0.82, corresponding to $T_{ex} \simeq 5 - 10$ K, typical of Galactic GMCs. Densities and kinetic temperatures obtained from LVG modeling indicate that the central GMCs have $\langle n_{H_2} \rangle \gtrsim 200 \text{ cm}^{-3}$ and $T_k \gtrsim 25$ K.

Three methods are compared to estimate the mass of molecular hydrogen and hence assess the validity of the Galactic conversion factor in NGC 3077. The 1.3 mm dust continuum emission upper limits and the optical dust extinction methods both yield masses consistent with estimates based on the Galactic conversion factor. Virial masses are slightly higher but consistent with the CO masses, except for the two GMCs closest to the starburst, which are probably not in virial equilibrium. The Galactic conversion factor appears applicable to NGC 3077, consistent with its solar metallicity.

2.6 mm continuum emission is also detected coincident with the main $P\alpha$ nebula, between the two largest GMCs. The spectrum is flat from 2.6 mm to 5 cm establishing that the bulk of the radio continuum emission is thermal free-free emission. The strength of the continuum implies that the central starburst region has $N_{Ly\alpha} \simeq 3.7 \times 10^{52} \text{ s}^{-1}$ or ~ 3000 O7 stars, 5 - 10 times that predicted from $H\alpha$ emission. Based on the continuum data an extinction-free star formation rate of $0.4 M_\odot \text{ yr}^{-1}$ is derived for the central 190 pc of NGC 3077. At this rate the amount of molecular gas present can sustain star formation for only ~ 10 Myrs. This age is consistent with the age of the superbubbles. We suggest that the burst is much younger than the age of the M 81-NGC 3077 interaction. (1) The youth of the burst, (2) the location of the burst at the interface between two GMCs, (3) the presence of molecular clouds distributed along the minor axis, and (4) the large amounts of atomic and molecular gas just outside the optical galaxy all lead to the conclusion that the current burst resulted from neutral gas that was torn out of the galaxy, raining back down on the disk. Dynamical considerations suggest that recently discovered molecular complex to the southeast of the galaxy is bound will also fall back into NGC 3077 rather than become a new dwarf

galaxy.

We are grateful to the faculty, staff and postdocs at OVRO for their support and assistance during the observations. We thank an anonymous referee for providing comments that help improve the paper. This work is supported in part by NSF grant AST-0071276. The Owens Valley Millimeter Interferometer is operated by Caltech with support from the NSF.

REFERENCES

- Abdel-Hamid, H. & Notni, P. 2000a, preprint (astro-ph/0011085)
- Abdel-Hamid, H. & Notni, P. 2000b, preprint (astro-ph/0011087)
- Appleton, P. N., Davies, R. D. & Stephenson, R. J. 1981, MNRAS, 195, 327
- Arimoto, N., Sofue, Y. & Tsujimoto, T. 1996, PASJ, 48, 275
- Arnault, P., Casoli, F., Combes, F., & Kunth, D. 1988, A&A, 205, 41
- Barbieri, C., Bertola, F. & di Tullio, G. 1974, A&A, 35, 463
- Barnes, J. E. & Hernquist, L. 1992, ARA&A, 30, 705
- Barone, L. T., Heithausen, A., Hüttemeister, S., Fritz, T. & Klein, U. 2000, MNRAS, 317, 649
- Beck, S. C. 2000, Sci Am, 282, 46
- Becker, B., Schilke, P. & Henkel, C. 1989, A&A, 211, L19
- Benacchio, L. & Galletta, G. 1981, ApJ, 243, L65
- Binney, J. & Tremaine, S., 1987, Galactic Dynamics, (Princeton: Princeton Univ. Press)
- Bohlin, R. C., Savage, B. D. & Drake, J. F. 1978, ApJ, 224, 132
- Böker, T. et al. 1999, ApJS, 124, 95
- Bothun, G. D., Lonsdale, C., J. & Rice, W. 1989, ApJ, 341, 129
- Braine, J. & Combes, F. 1992, A&A, 264, 433
- Brouillet, N., Baudry, A., Combes, F., Kaufman, K. & Bash, F. 1991, A&A, 242, 35
- Cernicharo, J., Bachiller, R. & Duvert, G. 1985, A&A, 149, 273
- Cottrell, G. A. 1976, MNRAS, 174, 455
- Crutcher, R. D., Rogstad, D. H. & Chu, K. 1978, ApJ, 225, 784

- De Jong, T., Chu, S.-I., & Dalgarno, A. 1975, *ApJ*, 199, 69
- de Vaucouleurs, G., de Vaucouleurs, A., & Corwin, H. G 1976, *Second Reference Catalog of Bright Galaxies* (Austin:Unvi. Texas Press)
- Donner, K. J. & Thomasson, M. 1993, *A&A*, 279, 28
- Elmegreen, B. G., 1989, *ApJ*, 338, 178
- Frerking, M A., Langer, W. D., & Wilson, R. W. 1982, *ApJ*, 262, 590
- Goldreich, P., & Kwan, J. 1974, *ApJ*, 189, 441
- Heckman, T. M. 1980, *A&A*, 87, 142
- Heithausen, A. & Walter, F. 2000, *A&A*, 361, 530
- Hernquist, L. 1989, *Nature*, 340, 687
- Hummel, E., van der Hulst, J. M., Keel, W. C. & Kennicutt Jr., R. C. 1987, *A&AS*, 70, 517
- Hunter, S. D. et al. 1997, *ApJ*, 481, 205
- Israel, F. P. 1986, *A&A*, 168, 369
- Israel, F. P., De Gwaauw, Th., Van de Stadt, H. & De Vries, C. P. 1986, *ApJ*, 303, 186
- MacLaren, I., Richardson, K. M., & Wolfendale, A. W. 1988, *ApJ*, 333, 821
- Maloney, P., & Black, J. H. 1988, *ApJ*, 325, 389.
- Maoz, D., Fillipenko, A. V., Ho, L. C., Macchetto, F. D., Rix, H.-W. & Schneider, D. P. 1996, *ApJS*, 107, 215
- Martin, C. L. 1997, *ApJ*, 491, 561
- Martin, C. L. 1998, *ApJ*, 506, 222
- Meier, D. S., Hurt, R. L. & Turner, J. L. 2001, in prep.
- Meier, D. S. & Turner, J. L. 2001, *ApJ*, 551, 687
- Meier, D. S., & Turner, J. L. 1998, in: K.A. van der Hucht, G. Koenigsberger & P.R.J. Eenens (eds.), *Wolf-Rayet Phenomena in Massive Stars and Starburst Galaxies*, *Proc. IAU Symp.* No. 193 (San Francisco: ASP), 746
- Meier, D. S., Turner, J. L., Crosthwaite, L. P. & Beck, S. C. 2001, *AJ*, 121, 740
- Melisse, J. P. M. & Israel, F. P. 1994, *A&AS*, 103, 391

- Meurer, G. R., Heckman, T. M., Leitherer, C., Kinney, A., Robert, C. & Garrett, D. R. 1995, *AJ*, 110, 2665
- Mezger, P. G. & Henderson, A. P. 1967, *ApJ*, 147, 471
- Niklas, S., Klein, U., Braine, J., & Wielebinski, R. 1995, *A&AS*, 114, 21
- Noguchi, M. 1987, *MNRAS*, 228, 635
- Padin, S., Scott, S. L., Woody, D. P., Scoville, N. Z., Seling, T. V., Finch, R. P., Ciovanine, C. J., & Lowrance, R. P. 1991, *PASP*, 103, 461
- Pollack, J. B., Hollenbach, D., Beckwith, S., Simonelli, D. P., Roush, T. & Fong, W. 1994, *ApJ*, 421, 615
- Price, J., S. & Gullixson, C. A. 1989, *ApJ*, 337, 658
- O’Connell, R. C., Gallagher, J. S. & Hunter 1994, *ApJ*, 433, 65
- Oka, T., Hasegawa, T., Hayashi, M., Handa, T. & Sakamoto, S. 1998, *ApJ*, 493, 730
- Rownd, B. K. & Young, J. S. 1999, *AJ*, 118, 670
- Rubio, M., Lequeux, J. & Boulanger, F. 1993, *A&A*, 271, 9
- Sage, L. J., Salzer, J. J., Loose, H.-H. & Henkel, C. 1992, *A&A*, 265, 19
- Sakai, S. & Madore, B. F. 2001, preprint (astro-ph/0103121)
- Sakamoto, S. 1996, *ApJ*, 462, 215
- Sakamoto, S., Hasegawa, T., Hayashi, M., Handa, T. & Oka, T. 1997, *ApJ*, 486, 276
- Scoville, N. Z., Carlstrom, J., Padin, S., Sargent, A., Scott, S. & Woody, D. 1994, *Astronomy with Millimeter and Submillimeter Wave Interferometry*, IAU Colloquium 140, ASP Conference Series, Vol. 59, 1994, M. Ishiguro and J. Welch, Eds., p.10
- Scoville, N. Z., Sargent, A. I., Sanders, D. B. & Soifer, B. T. 1991, *ApJ*, 366, L5
- Scoville, N. Z. & Solomon, P. M. 1974, *ApJ*, 187, L67
- Scoville, N. Z., Yun, M. S., Clemens, D. P., Sanders, D. B. & Waller 1987, *ApJS*, 63, 821
- Sparke, L. S., & Gallagher, J. S. III 2000, "Galaxies in the Universe: An Introduction", (Cambridge: Cambridge University Press), 225
- Solomon, P. M., Rivolo, A. R., Barrett, J. W., & Yahil, A. 1987, *ApJ*, 319, 730
- Solomon, P. M., Downes, D., Radford, S. J. E. & Barrett, J. W. 1997, *ApJ*, 478, 144

- Sramek, R. 1975, *AJ*, 80, 771
- Strong, A. W. et al., 1988, *A&A*, 207, 1
- Taylor, C. L., Hüttemeister, S., Klein, U., & Greve, A. 1999, *A&A*, 349, 424
- Thomasson, M. & Donner, K. J. 1993, *A&A*, 272, 153
- Thronson Jr., H. A. & Carlstrom, J. 1992, in: the Third Teton Summer School: Evolution of Galaxies and Their Environments, ed. Schull, J. M., Thronson Jr, H. A. (Dordrecht:Kluwer), 189
- Thronson Jr., H. A., Wilton, C. & Ksir, A. 1991, *MNRAS*, 252, 543
- Turner, J. L. 1994, “Mass-Transfer Induced Activity in Galaxies”, ed. Shlosman, I. (Cambridge: Cambridge University Press), 90
- Turner, J. L., Beck, S. C. & Hurt R. L. 1997, *ApJ*, L474, 11
- Vacca, W. D. 1996, Garmany, C. D. & Shull, M. J. 1996*ApJ*, 460, 914
- Vacca, W. D., Robert, C., Leitherer, C. & Conti, P. S. 1995, *ApJ*, 444, 647
- van der Hulst, J. M. 1979, *A&A*, 75, 97
- Verter, F. & Hodge, P. 1995, *ApJ*, 446, 616
- Vogel, S. N., Boulanger, F. & Ball, R. 1987, *ApJ*, 321, L145
- Wakker, B. P. & van Woerden, H. 1997, *ARA&A*, 35, 217
- Walter, F. & Heithausen, A. 1999, *ApJ*, 519, L69
- Walter, F., Taylor, C. L., Hüttemeister, S., Scoville, N. Z. & McIntyre, V. 2001, *AJ*, 121, 727
- Walter, F., Weiss, A., Martin, C. L. & Scoville, N. Z. 2001, *AJ*, submitted
- Weiss, A., Neininger, N., Hüttemeister, S. & Klein, U. 2001, *A&A*, 365, 571
- Wiklind, T., Combes, F. & Henkel, C. 1995, *A&A*, 297, 643
- Wilson, C. D. 1994, *ApJ*, L434, 11
- Wilson, C. D. 1995, *ApJ*, L448, 97
- Wilson, C. D. & Rudolph, A. L. 1993, *ApJ*, 406, 477
- Wilson, C. D. & Scoville, N. Z. 1990, *ApJ*, 363, 435

- Wilson, C. D., Scoville, N. Z., Freedman, W. L., Madore, B. F., & Sanders, D. B. 1988, *ApJ*, 333, 611
- Young, J. S. & Devereux, N. A. 1991, *ApJ*, 373, 414
- Young, J. S. & Scoville, N. Z. 1984, *ApJ*, 287, 153
- Yun, M. S., in: IAU Symp. 186, *Galaxy Interactions at Low and High Redshift*, ed. Barnes, J. E., Sanders, D. B. (Dordrecht:Kluwer), 81
- Yun, M. S., Ho, P. T. P. & Lo, K. Y. 1993, *ApJ*, 411, L17
- Yun, M. S., Ho, P. T. P. & Lo, K. Y. 1994, *Nature*, 372, 530

Fig. 1.— CO(1-0) channel map. LSR velocities are listed at the top right of each plane. The contours are plotted in intervals of 55 mJy beam^{-1} (or 0.75 K for the $2.''9 \times 2.''3$ beam), corresponding to 2σ . The beam is plotted in the bottom left of the first plane.

Fig. 2.— CO(2-1) channel map. LSR velocities are listed at the top right of each plane. The contours are plotted in intervals of $0.11 \text{ Jy beam}^{-1}$ (0.38 K) corresponding to 2σ . The beamsize has been smoothed to the same resolution as the CO(1-0) data.

Fig. 3.— The integrated intensity of the two transitions. (a) CO(1-0) integrated intensity. The contours are in steps of the theoretical 2σ value of 8.9 K km s^{-1} . The fitted positions of the GMCs are labeled on plot. The location of the starburst is marked by the label, “S”, and the positions of the two UV clusters are also labeled. (b) CO(2-1) integrated intensity. Contours are in steps of the 3σ value of 8.6 K km s^{-1} . The large oval represents the FWHM power points of the mosaicked (2-1) field. The true map noise is slightly lower than the above quoted values since the channel maps were clipped at 1.2σ when making the integrated intensity maps.

Fig. 4.— The CO(1-0) integrated intensity overlaid on the HST images. (a) The CO(1-0) overlaid on the HST NICMOS F160W (H band) continuum image (Böker et al. 1999). The contours are the same as in Figure 3. (b) The CO(1-0) overlaid on the HST NICMOS F187N ($P\alpha$) image (Böker et al. 1999). For reference, the white asterisk marks the fitted centroid of the 2.6 mm continuum. (c) The CO(1-0) overlaid on the HST FOC F220W UV image (Maoz et al. 1996).

Fig. 5.— The velocity field as measured from the CO(1-0) data. (a) The velocity field (moment 1 map) of NGC 3077. Contours are in steps of 5 km s^{-1} , with dashed contours representing negative velocities. The greyscale runs from -27 km s^{-1} to $+27 \text{ km s}^{-1}$. The bold dashed line marks the major axis of the galaxy. The two bold ticks mark the 0 km s^{-1} contour. The insert displays the rotation curve taken along the major axis (dotted line). (b) The velocity dispersion (moment 2) map. Contours are in increments of 5 km s^{-1} . The greyscale runs from 0 km s^{-1} to $+21 \text{ km s}^{-1}$.

Fig. 6.— The 2.6 mm continuum image. The 112 GHz continuum map displayed with a $75\text{k}\lambda$ taper. Contours are in steps of the 2σ value of $2.5 \text{ mJy beam}^{-1}$. Dashed contours represent negative values. The beam is plotted in the lower left.

Fig. 7.— The LVG modeling for (a) GMC D, (b) GMC B, and (c) GMC A of NGC3077. Contoured regions represent 1σ confidence solutions for the observed CO(1-0) antenna temperature and the CO(2-1)/CO(1-0) temperature ratio. Asterisks mark the location of the best fit (minimum χ^2). Gray lines are the solutions for a representative value of $X_{12\text{CO}}/dv/dr = 10^{-4.1}$, which corresponds to a solar $[\text{CO}/\text{H}_2]$ abundance of 8×10^{-5} and a velocity gradient of $1 \text{ km s}^{-1} \text{ pc}^{-1}$, consistent with the data, Table 4. Black lines represent a lower metallicity / higher velocity gradient model with $X_{12\text{CO}}/dv/dr = 10^{-4.5}$ for comparison. The fitted models assume a filling factor of 0.5 for GMCs B & D and a filling factor of 0.2 for GMC A (see text). Increasing the filling factor to unity will push the best fit solutions towards slightly lower kinetic temperatures and slightly higher densities. The dot-dashed line shows the beam-averaged densities implied if each GMC is in virial equilibrium

(Table 4).

Table 1. NGC 3077 Basic Data

Characteristic	Value	Reference
Revised Hubble Class	I0pec	1
Dyn. Center	$\alpha(2000) = 10^h03^m19.^s16$ $\delta(2000) = +68^\circ44'01''.4$	2
V_{lsr}	5.0 km s ⁻¹	2
Adopted Distance	3.9 Mpc	3
Major Axis P.A.	45°	4
L_{IR}	$7.2 \times 10^8 M_\odot^a$	4
M_{HI}	$3.6 \times 10^8 M_\odot^{a,b}$	5
$N_{Lyc}(2.6 \text{ mm})$	$3.7 \times 10^{52} s^{-1}$	2
SFR(H α)	$0.06 M_\odot yr^{-1a}$	6,7
SFR(Ext. Corrected)	$0.4 M_\odot yr^{-1a}$	2

^aCorrected for the adopted distance

^bInside the Holmberg Radius

Note. — Units of right ascension are hours, minutes and seconds, and units of declination are degrees, arcminutes, and arcseconds.

References. — (1) de Vaucouleurs, de Vaucouleurs & Corwin 1976; (2) this paper; (3) Sakai & Madore 2001; (4) Melisse & Israel 1994; (5) van der Hulst 1979; (6) Becker et al. 1989; (7) Thronson et al. 1991

Table 2. Observational Data^a

Transition ^b	Frequency (GHz)	ΔV_{chan} (km s ⁻¹)	$\Delta \nu_{band}$ (MHz)	Beamsize (arcsec; deg)	Noise level (mK / mJy Bm ⁻¹)
CO(1-0)	115.271	5.21	128	$2.9 \times 2.3; -68^\circ$	380/28
CO(2-1)	230.538	5.20 ^c	128	$2.9 \times 2.3; -68^\circ$ ^d	190/55
3mm Cont. ^e	112.1	...	1000	$3.0 \times 2.3; -81^\circ$	6.9 / 0.7
1mm Cont.	230.7	...	1000	$3.0 \times 2.3; -81^\circ$ ^d	8.3/2.5

^aFor observations made from 1997 October 12 - 1997 December 09

^bPhase Center #1: $\alpha = 10^h 03^m 19^s.23$ $\delta = +68^\circ 44' 03.''4$ (J2000)

Phase Center #2: $\alpha = 10^h 03^m 17^s.56$ $\delta = +68^\circ 44' 09.''4$ (J2000)

^cThe CO(2-1) maps were smoothed to 5.2 km s⁻¹ resolution from 2.6 km s⁻¹.

^dThe 1 mm maps are smoothed to the resolution of the 3 mm data.

^eFor the map displayed in Figure 6, a 75k λ taper is applied giving a beamsize of $3.''9 \times 3.''8; -79^\circ$

Table 3. Measured Intensities & Ratios

GMC	$T_{mb}(1-0)^a$ K	I_{CO10}^a (Kkms $^{-1}$)	$T_{mb}(2-1)^a$ K	I_{CO21}^a (Kkms $^{-1}$)	$\frac{I_{CO(2-1)}^b}{I_{CO(1-0)}}$	$\frac{T_{CO(2-1)}^b}{T_{CO(1-0)}}$
A	1.7	34	1.4	20	0.59 ± 0.15	0.82 ± 0.23
B	2.0	57	1.2	28	0.49 ± 0.12	0.60 ± 0.16
C	3.0	51	1.9	45	0.88 ± 0.20	0.63 ± 0.11
D	1.1	18	0.5	9	0.50 ± 0.22	0.45 ± 0.24
E	1.1	19	0.8	16	0.84 ± 0.30	0.73 ± 0.38
F	3.0	27
G	2.6	29

^aUncertainties are based on the larger of the statistical noise or the absolute calibration uncertainty, and are $\simeq 10\%$ for (1-0) and $\simeq 20\%$ for (2-1).

^bThe displayed ratios are not corrected for differences in resolved out flux. Assuming the resolved out flux is constant over the map, the true ratios should be corrected up by a factor of $0.77/0.58 = 1.33$.

Table 4. Giant Molecular Clouds in NGC 3077

GMC ^a	α_o, δ_o^e	$a \times b$ ($pc \times pc$)	$\Delta v_{1/2}$ (km/s)	M_{vir} ($10^6 M_\odot$)	$< n_{H_2} >^b$ ($10^3 cm^{-3}$)	M_{Xco}^c ($10^6 M_\odot$)
A	(20.24,03.2)	77×19	23	2.7	5.4	1.0
B	(19.08,00.1)	68×23	51	14	6.3	2.3
C	(18.88,51.3)	$< 10 \times < 10^f$	23	< 0.70	> 7.6	0.14
D	(18.85,57.8)	79×62	34	11	0.9	1.0
E	(16.3,08)	0.35
F	(13.71,09.8)	110×84	12	1.8	0.02	1.1
G	(12.6,17)	0.66

^aBased on fits to the CO(2-1) data, except GMC B which is fit with the CO(1-0) data.

^bThe average density is taken to be $M_{vir}/m_{H_2}Vf^{3/2}$ with $V = (4\pi/3)(0.7\sqrt{ab})^3$. f is assumed to be unity for GMC B.

^cBased on CO(1-0) with $X_{CO} = 2.3 \times 10^{20} cm^{-2} (K km s^{-1})^{-1}$, and corrected for resolved out flux.

^eBased on $(10^h 03^m; 68^o 44')$ for all GMCs except D and E, and $(10^h 03^m; 68^o 43')$ for D & E.

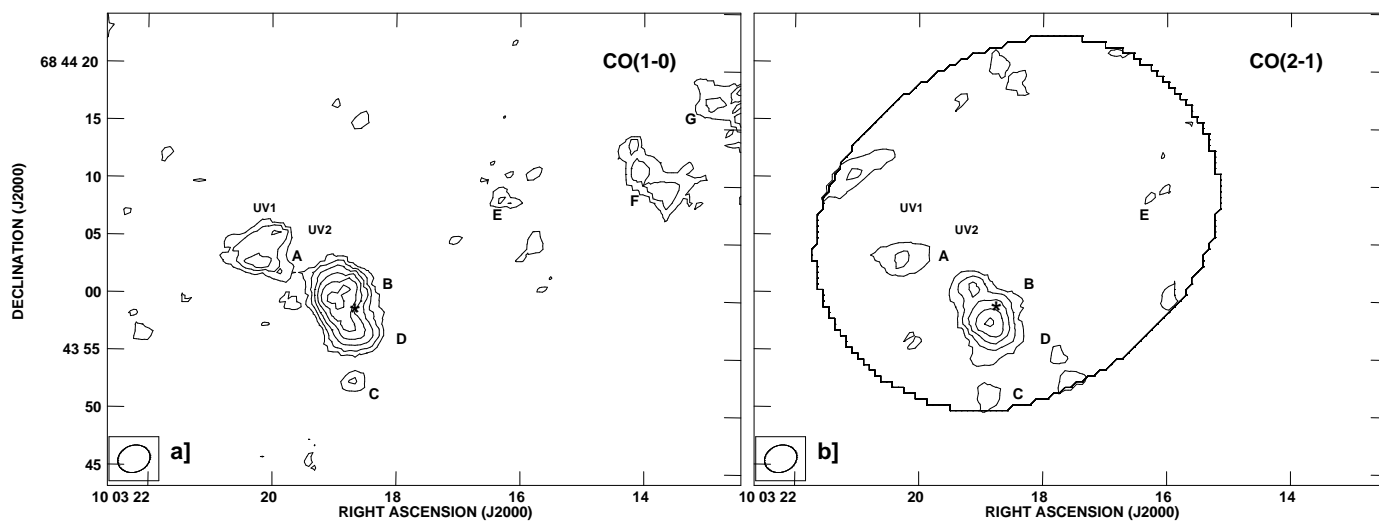
^fClouds are considered unresolved if the gaussian fit is smaller than 1/2 the beam minor axis ($\simeq 10 pc$).

This figure "meier.fig1.jpg" is available in "jpg" format from:

<http://arxiv.org/ps/astro-ph/0107031v1>

This figure "meier.fig2.jpg" is available in "jpg" format from:

<http://arxiv.org/ps/astro-ph/0107031v1>



This figure "meier.fig4.jpg" is available in "jpg" format from:

<http://arxiv.org/ps/astro-ph/0107031v1>

